Nano Research

ISSN 1998-0124 CN 11-5974/O4
https://doi.org/10.1007/s12274-019-2439-z

Research Article

Single Pt atom decorated graphitic carbon nitride as an efficient photocatalyst for the hydrogenation of nitrobenzene into aniline

Tianwei He, Chunmei Zhang, Lei Zhang, and Aijun Du (✉)

School of Chemistry, Physics and Mechanical Engineering, Science and Engineering Faculty, Queensland University of Technology, Gardens Point Campus, Brisbane, QLD 4001, Australia

© Tsinghua University Press and Springer-Verlag GmbH Germany, part of Springer Nature 2019

Received: 14 January 2019 / **Revised:** 14 May 2019 / **Accepted:** 17 May 2019

ABSTRACT

The hydrogenation of nitrobenzene into aniline is one of industrially important reactions, but still remains great challenge due to the lack of highly active, chemo-selective and eco-friendly catalyst. By using extensive density functional theory (DFT) calculations, herein we predict that single Pt atom decorated g-C_3N_4 (Pt@g-C_3N_4) exhibits excellent catalytic activity and selectivity for the conversion of nitrobenzene into aniline under visible light. The overall activation energy barrier for the hydrogenation of nitrobenzene on single atom Pt@g-C_3N_4 catalyst is even lower than that of the bare Pt(111) surface. The dissociation of N–O bonds on single Pt atom is triggered by single hydrogen atom rather than double hydrogen atoms on the Pt(111) surface. Moreover, the Pt@g-C_3N_4 catalyst exhibits outstanding chemoselectivity towards the common reducible substituents, such as phenyl, –C=C, –C≡C and –CHO groups during the hydrogenation. In addition, the doped single Pt atom can significantly enhance the photoconversion efficiency by broadening the light absorption of the pristine g-C_3N_4 to visible light region. Our results highlight an interesting and experimentally synthesized single-atom photocatalyst (Pt@g-C_3N_4) for efficient hydrogenation of nitrobenzene to aniline under a sustainable and green approach.

KEYWORDS

chemoselective hydrogenation, single-atom catalyst, photocatalyst, nitrobenzene

1 Introduction

Hydrogenation is among the most important and challenging technological reactions in modern chemical industry [1]. The high activity and chemoselectivity are often very difficult to control especially when more than one reducible groups are present during the hydrogenation process [2, 3]. An important example is the catalytic hydrogenation of nitrobenzene into aniline, a high-value chemical raw material which can be widely used in dyes, pigments, rubber, agrochemical and pharmaceutical industry [4, 5]. Currently, the catalytic hydrogenation of nitro groups to produce anilines mainly relies on noble metal complexes catalysts, such as palladium, rhodium, ruthenium and iridium [6, 7]. Although the precious metals have the advantage of high catalytic activity, they still suffer from low selectivity and high expense. Therefore, the exploration of environmentally benign and cost effective catalysts for aniline synthesis is thus of great fundamental as well as practical interest [8–10].

Great research efforts toward improving the activity and selectivity has been made by developing a variety of catalysts: noble metal catalysts Au [9, 11, 12], AuPt [13], CoPd [14], Pd/CeO_2 [2], non-noble metal catalysts Ni [15], Ni–Co as well as Ni–Fe alloys [16, 17] and so on [18–20]. However, the problem often arising is that these catalysts have to be modified by additives or combining with other metal oxides and molecules to achieve high selectivity [21–24]. In most cases, the well-chosen additives will cause environmental problems and at the same time reduce their activity [25]. Very recently, cobalt or iron based complexes catalysts have been developed as inexpensive catalysts with excellent chemoselectivities for the hydrogenation of nitroarens, but the reaction conditions are relatively demanding with more than 12 h reaction time, high temperature and high hydrogen pressure [26, 27]. In order to find a more gentle and economical protocol, some researchers tend to use semiconductor photocatalysts such as the metal nanoparticles or clusters (Au/TiO_2, Au/ZrO_2, Ag/g-C_3N_4 and CdS/g-C_3N_4) [28–33]. Some of them demonstrated excellent performance in degradation of organic pollutants and various organic transformations [34]. However, hydrogen atoms can easily diffuse to the subsurface region of metal nanoparticles or clusters during the hydrogenation reaction and the formed sub-hydrogen atoms could cause over-hydrogenation of the intermediates and thus lower the selectivity towards the desired products [35, 36]. Interestingly, some studies have revealed that the chemoselectivity towards the hydrogenation of –C=C and –C≡C groups is highly sensitive to the particle size, while the hydrogenation of nitro groups appears to be size insensitive over metal nanoparticles [37]. Inspired by these results, we assume that we can tune the chemoselectivity by reducing the size of metal particles [24, 38]. The limitation for downsizing metal particles is to use isolate single atom on the supports, namely "single-atom catalyst (SAC)" [39]. Most recently, single atom catalysis has been extensively explored since the seminal work of Pt_1/FeO_x reported by Zhang and co-workers in 2011 [40]. The efficient use of the metals and superior activity are rendering SAC very popular in water-splitting [41–44], metal-air battery [45, 46], CO oxidation [40, 47], CO_2 reduction [48] and N_2 fixation [49, 50]. However, few works have been reported for the use of SACs in the selective hydrogenation reactions. The most related work is a single Pt and pseudo-single Pt atom supported on FeO_x as a highly active catalyst for hydrogenation of nitroaromatics proposed by Zhang's group [51]. Whereas, the improved catalytic activity in some

Address correspondence to aijun.du@qut.edu.au

degree compromised the chemoselectivity. Another interesting work is isolated Pd atoms onto the defective nanodiamond-graphene (Pd/ND@G) for selective hydrogenation of acetylene to ethylene [52]. The experiment results showed that Pd/ND@G exhibited great catalytic performance to convert acetylene to ethylene. Therefore, there still lack of a sustainable catalytic route to achieve both high yields and selectivity.

Experimentally, optically active graphitic carbon nitride (g-C_3N_4) has been widely used as an excellent substrate for the design of single-atom photocatalysts [53–55]. The best example is the single Pt atom supported on g-C_3N_4 which has been successfully fabricated in recent experiment, showing excellent photocatalytic performance [56]. Although some non-noble metal catalysts have been developed recently, Pt is still regarded as the dominant catalyst in the hydrogenation of various nitroaromatics due to its excellent catalytic properties [57, 58]. In this work, we for the first time propose to use single-atom Pt atom supported on g-C_3N_4 as a green single atom catalyst to address the activity, selectivity and economical issues during the hydrogenation of nitrobenzene into aniline. Our results indicate that the nitrobenzene can selectively adsorb on the Pt atom through the phenyl group and be further hydrogenated into aniline with a rather low activation barrier of 0.73 eV, which is even lower than that on the widely studied Pt(111) surface (0.75 eV) [59]. Meanwhile, unlike over Pt surfaces, the monodispersed Pt atom prevented the coupling of multiple reactants to form the azo-compounds as by-products due to the strong steric hindrance. Additionally, the Pt@g-C_3N_4 catalyst exhibits excellent selectivity towards some common reducible substituents, such as phenyl, –C=C, –C≡C and –CHO groups. Most importantly, the supported Pt atom can significantly extend the absorption edge of g-C_3N_4 to the visible light region which enables the photo-driven hydrogenation of nitrobenzene into aniline.

2 Computational methods

The Vienna *ab initio* simulation package (VASP) code was used to perform all the geometric optimizations and electronic structures calculations [60, 61]. The core-valence interactions were accounted by using the functional of generalized gradient approximation (GGA) in the Perdew–Burk–Emzerhof (PBE) form combined with the projector augmented wave (PAW) method [60, 62]. The spin-polarization was employed through all the calculations and the energy cutoff for plane-wave expansions was set to 500 eV. The electronic relaxation for self-consistency was set to 10^{-5} eV and the residual forces were limited to less than 0.01 eV/Å. A Monkhorst–Pack *k*-point mesh of 3 × 3 × 1 grid was used during the calculations. To avoid the interaction between two periodic units, the vacuum space was set to more than 15 Å. Density functional theory (DFT)+D3 was used to treat the long range van der Waals interaction. The climbing nudged elastic band (CI-NEB) method was adopted to search for the saddle point and the optimal reaction pathway [63, 64]. We have taken all the possible elementary reaction steps which may happen on the catalyst into consideration. The energies changes related to these reaction steps were calculated using the following equation

$$\Delta E = E_{\text{adsorbate+catalyst}} - E_{\text{catalyst}} - E_{\text{adsorbats}}$$

$E_{\text{adsorbate+catalyst}}$, E_{catalyst} and $E_{\text{adsorbats}}$ stand for the total energy of the Pt@g-C_3N_4 with adsorbate, Pt@g-C_3N_4 catalyst and isolate adsorbate, respectively.

3 Results and discussion

Single Pt atom can be stably anchored into the host cavity of g-C_3N_4 by coordinating with two N atoms, as shown in Fig. 1(a). The binding energy was calculated to be −3.15 eV, which is consistent with other reports [55, 65]. The adsorption mode of the reactants on the catalyst surface has a significant impact on the catalytic selectivity during the heterogeneous catalysis [24, 66]. Thus, we first investigated all the possible adsorption configurations of nitrobenzene on the Pt@g-C_3N_4 catalyst. The nitrobenzene can be adsorbed on the single Pt atom through two different types, one is via the phenyl-group and the other one is via nitro-group. Four different adsorption geometries including Pt-phenyl, Pt–O–O, Pt–C–N and Pt–N–O were taken into consideration. Geometry optimization was carried out and binding energies were calculated for all these configurations. For the Pt–C–N configuration, the nitrobenzene spontaneously changed to Pt-phenyl adsorption mode during the optimization. As shown in Figs. 1(b)–1(d), the Pt-phenyl configuration owns the lowest binding energy of −1.96 eV compared to −1.7 eV for Pt–O–O and −1.42 eV for Pt–N–O. Accordingly, nitrobenzene prefers to bind on the single Pt atom through phenyl group. We further calculated the differential charge densities of the Pt-phenyl adsorption mode, as shown in Fig. S1 in the Electronic Supplementary Material (ESM). The adsorption behavior of nitrobenzene on Pt atom is similar to that on the Pt (111) surface [67, 68]. There is a significant charge transfer between the Pt atom and nitrobenzene, indicating a strong interaction between the reactant and catalyst. There is a charge depletion around the Pt atom with 1.12 e^- lost, while charge was accumulated around the nitro-group with 0.99 e^- gained based on the Bader charge analysis [69]. These results clearly demonstrated that nitrobenzene can be stably adsorbed on the catalyst which is crucial for the subsequent hydrogenation reaction.

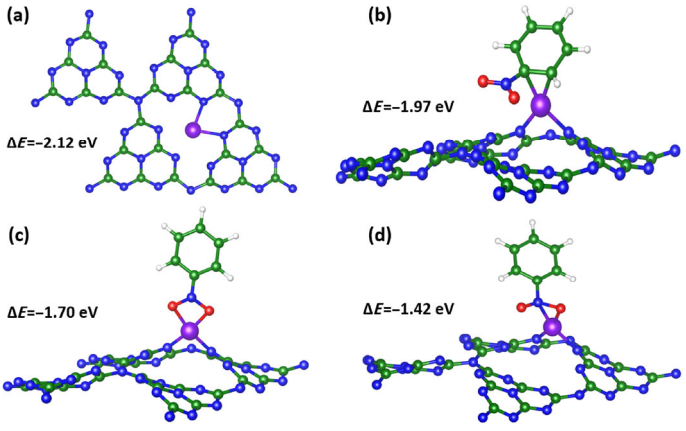

Figure 1 The top view of (a) the single Pt atom supported on g-C_3N_4 and side view of three typical adsorption configurations of (b) Pt-phenyl, (c) Pt–O–O and (d) Pt–N–O.

After figuring out the most stable adsorption configuration of nitrobenzene on the single Pt atom, we continue to investigate the hydrogenation reaction of the nitrobenzene (Ph-NO_2) to aniline (Ph-NH_2). The overall hydrogenation can be expressed as a six-electron process: $PhNO_2 + 6H^+ + 6e^- \rightarrow PhNH_2 + 2H_2O$. Two hydrogenation mechanisms were well known, i.e. the direct and condensation reaction pathways (see Scheme S1 in the ESM) as proposed by Haber in 1898 [70]. The difference between these two reaction pathways is whether azo-compounds can be formed during the hydrogenation reaction. Therefore, we first examined the possibility of the two reaction intermediates (*Ph-NO and *Ph-NHOH) interacting with each other to generate *Ph-N → NO-Ph* intermediate. The optimized structure showed that *Ph-NO intermediate could not bind with *Ph-NHOH intermediate due to the large distance between the adjacent active sites. Moreover, unlike the metal clusters or surfaces which could provide sufficient active sites for the co-adsorption of more than one nitrobenzene molecules, single atom active site can only adsorb one nitrobenzene molecule at one time due to the large steric hindrance. Under this circumstance, it is very hard for the intermediates to couple into azo-compounds on single Pt atom as by-products and thus production efficiency of aniline could be

greatly improved. Therefore, single atom Pt@g-C_3N_4 catalyst could offer significant advantage over the metal cluster or surface. In the following, we specifically investigated the direct reaction routes as shown in Scheme 1.

We then move to investigate the catalytic activity of single atom Pt@g-C_3N_4 catalyst for the conversion of nitrobenzene into aniline. The reaction process mainly involves the dissociation of N–O bonds and the formation of N–H bonds while accompanying by the generation of two water molecules as the by-products. As we can see from the Scheme 1, four possible reaction pathways will be fully explored to identify the most appropriate route. The calculated reaction energies and the activation energies for all the possible intermediates are summarized in Table 1. Notably, most reaction energies are negative and the most positive one is only 0.28 eV, suggesting favorable thermodynamic for the hydrogenation of nitrobenzene into aniline on the Pt@g-C_3N_4 catalyst. Then we calculated the activation barrier for every reaction step using the NEB method. The energy profiles for the most optimal reaction pathway are presented in Fig. 2. All the other three less favorable routes are included in Figs. S2–S4 in the ESM. For all the four reaction pathways, the first step for hydrogenation of nitro-group is that one proton–electron pair attacks on one of the O atoms to form *Ph-NOOH intermediate, which is basically an uphill reaction with a small positive reaction energy of 0.28 eV and needs to overcome a low activation barrier of 0.48 eV. The next proton–electron pair can either bind with another O atom to form *Ph-$(OH)_2$ intermediate or attack the newly formed OH group to generate a H_2O molecule. It is apparent that the reaction pathway with the broken N–O bond is more preferred with quite negative reaction energies (–1.66 eV vs. –0.48 eV) and small activation barriers (0.24 eV vs. 0.46 eV). Such low activation barriers mainly attribute to the adsorption of H atom that elongated the length of N–O bond from 1.21 to 1.42 Å and thus facilitated the dissociation of N–O bond to generate a H_2O molecule. Next, the third proton–electron pair comes up to bond with the O atom to form *Ph-NOH intermediate with an ultralow barrier of 0.09 eV. The fourth proton–electron pair will either combine with the N atom or break the second N–O bond. The calculated reaction energies for the formation of *Ph-NHOH and *Ph-N intermediates are 0.15 and –0.95 eV, respectively, suggesting the *Ph-NOH → *Ph-NHOH reaction path may be more difficult to occur than the *Ph-NOH → *Ph-N + H_2O path. The former reaction path needs to overcome a higher activation barrier of 0.99 eV (*Ph-NOH → *Ph-NHOH) compared to 0.73 eV for the later one (*Ph-NOH → *Ph-N + H_2O). Hence the preferred reaction path in this step is to break the second N–O bond and releasing another H_2O molecule. This reaction (*Ph-NOH → *Ph-N + H_2O) was the overall rate-determining step during the whole hydrogenation reaction. It is worth noting that previous works also revealed that the dissociation of N–O bonds is the key step during the reduction of nitro-group [59, 71, 72]. With another two proton–electron pairs get transferred, the nitrobenzene was eventually converted into aniline. Additional, the over hydrogenation of the produced aniline was also considered that we further undertook the NEB calculations to get the hydrogenation barrier [73]. The activation barrier (1.63 eV) of hydrogenation aniline is higher than desorption of aniline (1.1 eV), revealing that the over hydrogenation of aniline is not favorable.

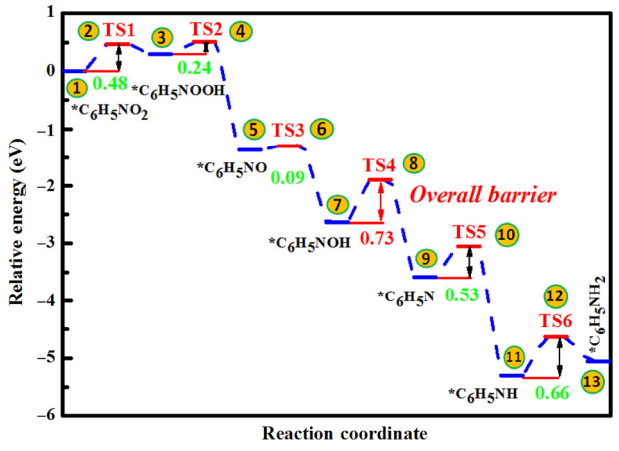

Figure 2 Energy profiles of the optimal reaction pathway for the hydrogenation of nitrobenzene into aniline on single atom Pt@g-C_3N_4 catalyst.

Figure 3 presented all the optimized reaction intermediates (odd-numbered configurations) and the transition states (even-numbered configurations) along the most favorable hydrogenation reaction

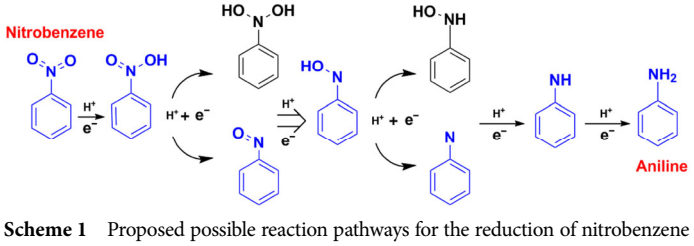

Scheme 1 Proposed possible reaction pathways for the reduction of nitrobenzene into aniline through direct routes (the reaction pathway in blue is the optimal one).

Table 1 Calculated reaction energies (ΔE, in eV) and activation barriers (E_a, in eV) of the elementary reaction steps involved the hydrogenation of nitrobenzene to aniline on the Pt/C_3N_4 catalyst

Reactions	ΔE	E_a
$C_6H_5NO_2$ + H → *C_6H_5NOOH	0.28	0.48
C_6H_5NOOH + H → *$C_6H_5N(OH)_2$	–0.48	0.46
C_6H_5NOOH + H → *C_6H_5NO +H_2O	–1.66	0.24
$C_6H_5N(OH)_2$ + H → *C_6H_5NOH +H_2O	–2.42	0.19
C_6H_5NO + H → *C_6H_5NOH	–1.25	0.09
C_6H_5NOH + H → *C_6H_5N +H_2O	–0.95	0.73
C_6H_5NOH + H → *C_6H_5NHOH	0.15	0.99
C_6H_5NHOH + H → *C_6H_5NH +H_2O	–2.83	1.18
C_6H_5N + H → *C_6H_5NH	–1.72	0.53
C_6H_5NH + H → *$C_6H_5NH_2$	0.24	0.66

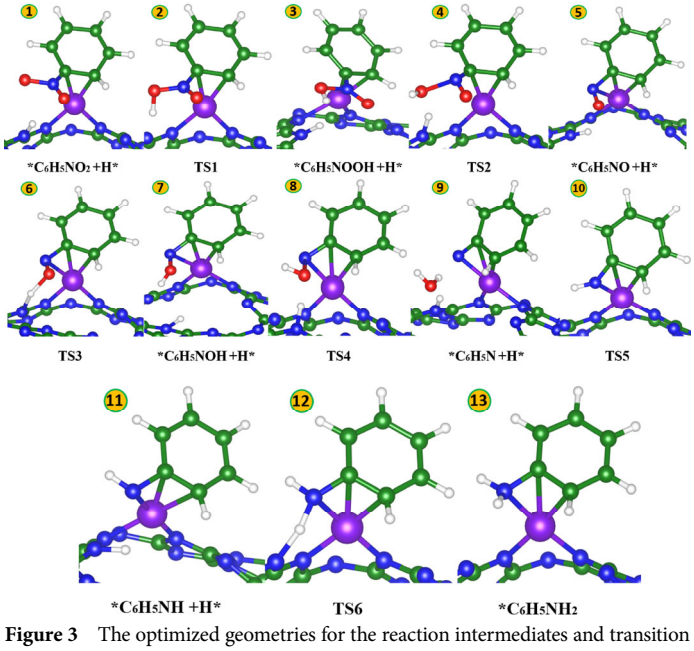

Figure 3 The optimized geometries for the reaction intermediates and transition states for the most favorable pathway shown in Fig. 2 during the hydrogenation process.

pathway (see Fig. 2). Here we focused more on examining the transition state geometries of the dissociations of two N–O bonds (TS2 and TS4). It was found that the N–O bonds were first elongated more than 0.2 Å when the first and third H* were transferred to O atom. That means the N–O bonds can be easily activated on the Pt@g-C_3N_4 catalyst by the adsorbed single proton. On the basis of reaction and activation energies shown in Table 1, the Ph-NOOH → Ph-NO → Ph-NOH → Ph-N pathway is more favorable than the reaction Ph-NOOH → Ph-$N(OH)_2$ → Ph-NOH → Ph-NHOH. Therefore, unlike conventional double H-induced reaction pathway on the Pt (111) surface [74], single hydrogen induced activation of N–O bond plays a more important role on the Pt@g-C_3N_4 catalyst during the deoxygenation reactions. Hence the mechanism for overall hydrogenation of nitrobenzene on the Pt@g-C_3N_4 catalyst can be identified as: Ph-NO_2 → Ph-NOOH → Ph-NO → Ph-NOH → Ph-N → Ph-NH → Ph-NH_2. The highest activation energy occurs at the dissociation of the second N–O bond (⑦ → ⑨ as shown in Fig. 2) with an activation energy barrier of 0.73 eV, which is even smaller than that on the Pt (111) surface. Thus the catalytic activity of single atom Pt@g-C_3N_4 is superior to that of the Pt (111) surface. More importantly, the use of single Pt atom significantly reduced the load of precious metal to the greatest extent.

Besides the high catalytic activity, the chemoselectivity is also another primary factor to evaluate the hydrogenation performance for single atom Pt@g-C_3N_4 catalyst. Generally some important nitroarenes during the organic synthesis are usually functionalized with a variety of other reducible groups [74]. These substituents will compete with the nitro-group and produce waste during the hydrogenation of nitrobenzene into aniline. For this reason, we further investigated the chemoselectivity of Pt@g-C_3N_4 catalyst towards some common reducible groups including phenyl, –C=C, –C≡C and –CHO substituents. The reaction pathways for hydrogenating these functional groups are depicted in Fig. 4. It can be clearly seen that the hydrogenations of phenyl, –C=C, –C≡C and –CHO substituents on single atom Pt@g-C_3N_4 catalyst possess remarkably high barriers of 1.05, 1.49, 1.29 and 1.53 eV, respectively. It is worth noting that the overall activation energy for the hydrogenation of nitrobenzene was only 0.73 eV. The large difference of the activation energy between the above reactions indicated the hydrogenation of nitrobenzene is highly feasible at the room temperature, while the hydrogenation of other phenyl, –C=C, –C≡C and –CHO substituents is rather difficult. Therefore, the overall hydrogenation reaction will give preference for the single Pt@g-C_3N_4 catalyst to attack the nitro-group to yield aniline products even in the presence of the above four reducible groups. This indicated an ideal high chemoselectivity for the hydrogenation of nitrobenzene into aniline, which is in sharp contrast with other widely studied metal cluster or surface catalysts where some environmentally-unfriendly additives are normally used to improve their chemoselectivity, but often at the price of sacrificing the catalytic activity to a great extent.

Experimentally, g-C_3N_4-based photocatalysts have been widely studied for energy conversion and pollutants degradation [75, 76]. The pristine g-C_3N_4 has a relatively large band gap of 2.7 eV, rendering minimal absorption of visible light [77]. As shown in Fig. 5, the light adsorption for the pristine g-C_3N_4 mainly located in the ultraviolet region. However, single Pt atom decorated g-C_3N_4 could significantly improve the optical absorption activity (see Fig. 5). The light absorption of the Pt@g-C_3N_4 composite can be extended to the visible and infrared light region due to a narrowed band gap (0.72 eV) [55]. Therefore, the Pt@g-C_3N_4 catalyst is able to hydrogenate nitrobenzene into aniline under visible/infrared light irradiation compared to the pure g-C_3N_4 catalyst.

4 Conclusions

In summary, we propose a novel single atom photocatalyst, Pt@g-C_3N_4, with outstanding photo-catalytic activity and chemoselectivity for the hydrogenation of nitrobenzene into aniline. The optimal hydrogenation pathway is identified as: Ph-NO_2 → Ph-NOOH → Ph-NO → Ph-NOH → Ph-N → Ph-NH → Ph-NH_2. The most energy demanding step among the hydrogenation process is the dissociation of the second N–O bond with an activation barrier of 0.73 eV only. The mechanism of single H-induced activation of N–O bond plays a crucial role in the hydrogenation reaction. Moreover, activation

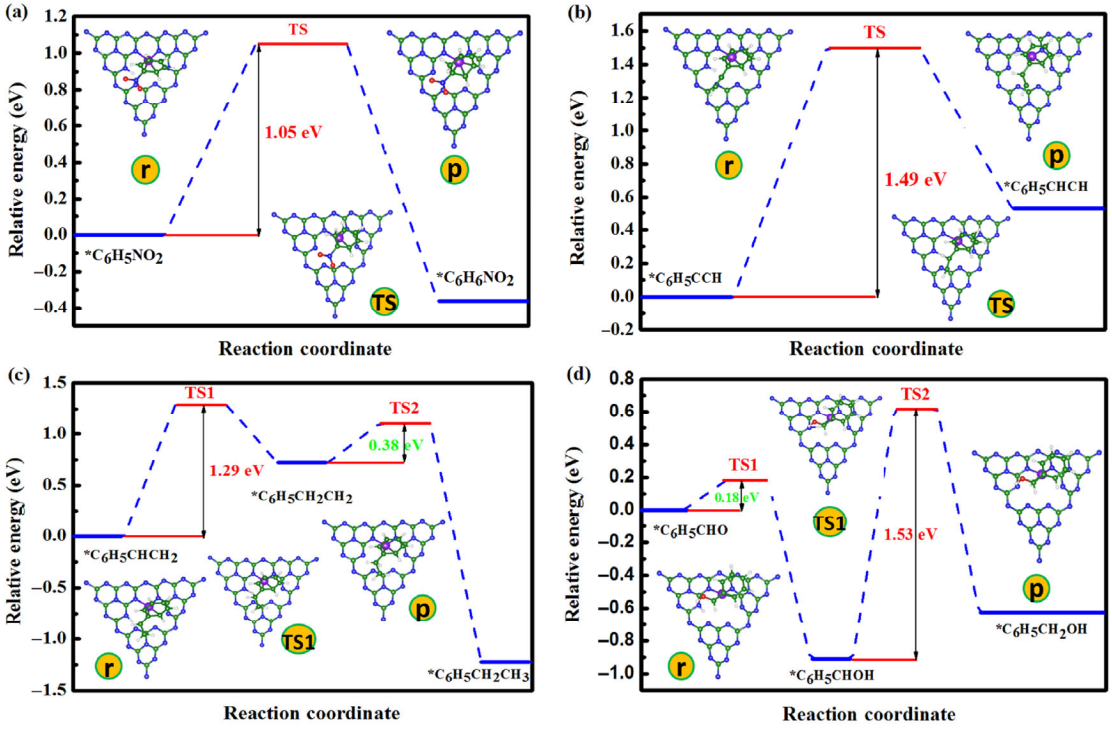

Figure 4 Energy profiles for the hydrogenation of phenyl, –C=C, –C≡C and –CHO substituents on single atom Pt@g-C_3N_4 catalyst. Insets are the structures of reactants, products and transition states during the hydrogenation process. The green, blue, purple and white balls represent C, N, Pt and H atoms, respectively.

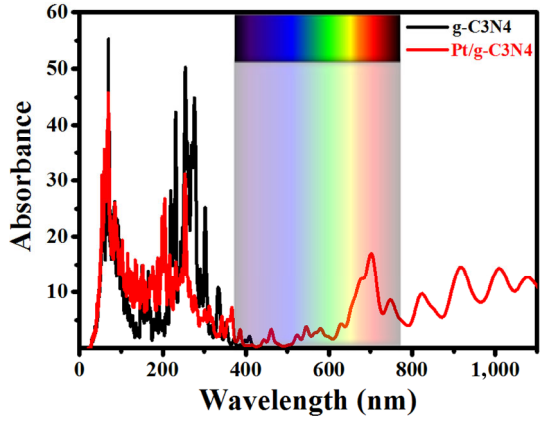

Figure 5 The optical absorption spectra for the pristine g-C_3N_4 and the Pt/g-C_3N_4.

barriers for hydrogenation of phenyl, –C=C, –C≡C and –CHO substituents are rather high compared with the nitro-group, indicating that single atom Pt@g-C_3N_4 catalyst possesses excellent chemoselectivities towards various reducible groups. Additionally, single Pt atom supported on g-C_3N_4 can greatly broaden the range of light absorption, allowing the hydrogenation of nitrobenzene into aniline to be driven under visible/infrared light. The high catalytic activity, outstanding selectivity towards various reducible groups, excellent photocatalytic performance and efficient use of the noble metal render Pt@g-C_3N_4 a promising environmentally benign single atom photocatalyst for the hydrogenation of nitrobenzene into aniline.

Acknowledgements

We acknowledge generous grants of high-performance computing resources provided by NCI National Facility and The Pawsey Supercomputing Centre through the National Computational Merit Allocation Scheme supported by the Australian Government and the Government of Western Australia. A. D. also greatly appreciates the financial support of the Australian Research Council under Discovery Project (No. DP170103598).

References

[1] Zhao, M. T.; Yuan, K.; Wang, Y.; Li, G. D.; Guo, J.; Gu, L.; Hu, W. P.; Zhao, H. J.; Tang, Z. Y. Metal–organic frameworks as selectivity regulators for hydrogenation reactions. *Nature*, **2016**, *539*, 76–80.

[2] Zhang, S.; Chang, C. R.; Huang, Z. Q.; Li, J.; Wu, Z. M.; Ma, Y. Y.; Zhang, Z. Y.; Wang, Y.; Qu, Y. Q. High catalytic activity and chemoselectivity of sub-nanometric Pd clusters on porous nanorods of CeO_2 for hydrogenation of nitroarenes. *J. Am. Chem. Soc*. **2016**, *138*, 2629–2637.

[3] Beier, M. J.; Andanson, J. M.; Baiker, A. Tuning the chemoselective hydrogenation of nitrostyrenes catalyzed by ionic liquid-supported platinum nanoparticles. *ACS Catal*. **2012**, *2*, 2587–2595.

[4] Marquez, J.; Pletcher, D. A study of the electrochemical reduction of nitrobenzene to p-aminophenol. *J. Appl. Electrochem*. **1980**, *10*, 567–573.

[5] Corma, A.; Concepción, P.; Serna, P. A different reaction pathway for the reduction of aromatic nitro compounds on gold catalysts. *Angew. Chem., Int. Ed*. **2007**, *46*, 7266–7269.

[6] Joshi, R.; Chudasama, U. Hydrogenation and oxidation reactions involving ruthenium supported catalysts. *Ind. Eng. Chem. Res*. **2010**, *49*, 2543–2547.

[7] Deshmukh, A. A.; Prashar, A. K.; Kinage, A. K.; Kumar, R.; Meijboom, R. Ru(II) phenanthroline complex as catalyst for chemoselective hydrogenation of nitro-aryls in a green process. *Ind. Eng. Chem. Res*. **2010**, *49*, 12180–12184.

[8] Noyori, R. Synthesizing our future. *Nat. Chem*. **2009**, *1*, 5–6.

[9] Corma, A.; Serna, P. Chemoselective hydrogenation of nitro compounds with supported gold catalysts. *Science* **2006**, *313*, 332–334.

[10] Wienhöfer, G.; Sorribes, I.; Boddien, A.; Westerhaus, F.; Junge, K.; Junge, H.; Llusar, R.; Beller, M. General and selective iron-catalyzed transfer hydrogenation of nitroarenes without base. *J. Am. Chem. Soc*. **2011**, *133*, 12875–12879.

[11] He, D. P.; Shi, H.; Wu, Y.; Xu, B. Q. Synthesis of chloroanilines: Selective hydrogenation of the nitro in chloronitrobenzenes over zirconia-supported gold catalyst. *Green Chem*. **2007**, *9*, 849–851.

[12] He, L.; Wang, L. C.; Sun, H.; Ni, J.; Cao, Y.; He, H. Y.; Fan, K. N. Efficient and selective room-temperature gold-catalyzed reduction of nitro compounds with CO and H_2O as the hydrogen source. *Angew. Chem., Int. Ed*. **2009**, *48*, 9538–9541.

[13] Serna, P.; Concepción, P.; Corma, A. Design of highly active and chemoselective bimetallic gold–platinum hydrogenation catalysts through kinetic and isotopic studies. *J. Catal*. **2009**, *265*, 19–25.

[14] Shen, K.; Chen, L.; Long, J. L; Zhong, W.; Li, Y. W. MOFs-templated Co@Pd core–shell nps embedded in N-doped carbon matrix with superior hydrogenation activities. *ACS Catal*. **2015**, *5*, 5264–5271.

[15] Ren, Y. J.; Wei, H. S.; Yin, G. Z.; Zhang, L. L.; Wang, A. Q.; Zhang, T. Oxygen surface groups of activated carbon steer the chemoselective hydrogenation of substituted nitroarenes over nickel nanoparticles. *Chem. Commun*. **2017**, *53*, 1969–1972.

[16] Liu, L. C.; Gao, F.; Concepción, P.; Corma, A. A new strategy to transform mono and bimetallic non-noble metal nanoparticles into highly active and chemoselective hydrogenation catalysts. *J. Catal*. **2017**, *350*, 218–225.

[17] Zhang, J. W.; Lu, G. P.; Cai, C. Chemoselective transfer hydrogenation of nitroarenes by highly dispersed Ni-Co BMNPs. *Catal. Commun*. **2016**, *84*, 25–29.

[18] Daems, N.; Wouters, J.; Van Goethem, C.; Baert, K.; Poleunis, C.; Delcorte, A.; Hubin, A.; Vankelecom, I. F. J.; Pescarmona, P. P. Selective reduction of nitrobenzene to aniline over electrocatalysts based on nitrogen-doped carbons containing non-noble metals. *Appl. Catal. B: Environ*. **2018**, *226*, 509–522.

[19] Sheng, X.; Wouters, B.; Breugelmans, T.; Hubin, A.; Vankelecom, I. F. J.; Pescarmona, P. P. Cu/Cu_xO and Pt nanoparticles supported on multi-walled carbon nanotubes as electrocatalysts for the reduction of nitrobenzene. *Appl. Catal. B: Environ*. **2014**, *147*, 330–339.

[20] Nguyen, T. B.; Huang, C. P.; Doong, R. A. Enhanced catalytic reduction of nitrophenols by sodium borohydride over highly recyclable Au@graphitic carbon nitride nanocomposites. *Appl. Catal. B: Environ*. **2019**, *240*, 337–347.

[21] Raja, R.; Golovko, V. B.; Thomas, J. M.; Berenguer-Murcia, A.; Zhou, W. Z.; Xie, S. H.; Johnson, B. F. G. Highly efficient catalysts for the hydrogenation of nitro-substituted aromatics. *Chem. Commun*. **2005**, 2026–2028.

[22] Blaser, H. U.; Steiner, H.; Studer, M. Selective catalytic hydrogenation of functionalized nitroarenes: An update. *ChemCatChem* **2009**, *1*, 210–221.

[23] Corma, A.; González-Arellano, C.; Iglesias, M.; Sánchez, F. Gold complexes as catalysts: Chemoselective hydrogenation of nitroarenes. *Appl. Catal. A: Gen*. **2009**, *356*, 99–102.

[24] Corma, A.; Serna, P.; Concepción, P.; Calvino, J. J. Transforming nonselective into chemoselective metal catalysts for the hydrogenation of substituted nitroaromatics. *J. Am. Chem. Soc*. **2008**, *130*, 8748–8753.

[25] Siegrist, U.; Baumeister, P.; Blaser, H. U.; Studer, M. The selective hydrogenation of functionalized nitroarenes: New catalytic systems. *Chem. Ind*. **1998**, *75*, 207–220.

[26] Westerhaus, F. A.; Jagadeesh, R. V.; Wienhöfer, G.; Pohl, M. M.; Radnik, J.; Surkus, A. E.; Rabeah, J.; Junge, K.; Junge, H.; Nielsen, M. et al. Heterogenized cobalt oxide catalysts for nitroarene reduction by pyrolysis of molecularly defined complexes. *Nat. Chem*. **2013**, *5*, 537–543.

[27] Jagadeesh, R. V.; Surkus, A. E.; Junge, H.; Pohl, M. M.; Radnik, J.; Rabeah, J.; Huan, H. M; Schünemann, V.; Brückner, A.; Beller, M. Nanoscale Fe_2O_3-based catalysts for selective hydrogenation of nitroarenes to anilines. *Science* **2013**, *342*, 1073–1076.

[28] Zhu, H. Y.; Ke, X. B.; Yang, X. Z.; Sarina, S.; Liu, H. W. Reduction of nitroaromatic compounds on supported gold nanoparticles by visible and ultraviolet light. *Angew. Chem., Int. Ed*. **2010**, *49*, 9657–9661.

[29] Naya, S. I.; Inoue, A.; Tada, H. Self-assembled heterosupramolecular visible light photocatalyst consisting of gold nanoparticle-loaded titanium(IV) dioxide and surfactant. *J. Am. Chem. Soc*. **2010**, *132*, 6292–6293.

[30] Li, H.; Qin, F.; Yang, Z. P.; Cui, X. M.; Wang, J. F.; Zhang, L. Z. New reaction pathway induced by plasmon for selective benzyl alcohol oxidation on biocl possessing oxygen vacancies. *J. Am. Chem. Soc.* **2017**, *139*, 3513–3521.
[31] Xiao, Q.; Liu, Z.; Wang, F.; Sarina, S.; Zhu, H. Y. Tuning the reduction power of visible-light photocatalysts of gold nanoparticles for selective reduction of nitroaromatics to azoxy-compounds—Tailoring the catalyst support. *Appl. Catal. B: Environ.* **2017**, *209*, 69–79.
[32] Yang, Z. W.; Xu, X. Q.; Liang, X. X.; Lei, C.; Cui, Y. H.; Wu, W. H.; Yang, Y. X.; Zhang, Z.; Lei, Z. Q. Construction of heterostructured MIL-125/Ag/g-C_3N_4 nanocomposite as an efficient bifunctional visible light photocatalyst for the organic oxidation and reduction reactions. *Appl. Catal. B: Environ.* **2017**, *205*, 42–54.
[33] Dai, X.; Xie, M. L.; Meng, S. G.; Fu, X. L.; Chen, S. F. Coupled systems for selective oxidation of aromatic alcohols to aldehydes and reduction of nitrobenzene into aniline using CdS/g-C_3N_4 photocatalyst under visible light irradiation. *Appl. Catal. B: Environ.* **2014**, *158-159*, 382–390.
[34] Hoffmann, M. R.; Martin, S. T.; Choi, W.; Bahnemann, D. W. Environmental applications of semiconductor photocatalysis. *Chem. Rev.* **1995**, *95*, 69–96.
[35] Tew, M. W.; Janousch, M.; Huthwelker, T.; Van Bokhoven, J. A. The roles of carbide and hydride in oxide-supported palladium nanoparticles for alkyne hydrogenation. *J. Catal.* **2011**, *283*, 45–54.
[36] García-Mota, M.; Bridier, B.; Pérez-Ramírez, J.; López, N. Interplay between carbon monoxide, hydrides, and carbides in selective alkyne hydrogenation on palladium. *J. Catal.* **2010**, *273*, 92–102.
[37] Zhao, F. Y.; Ikushima, Y.; Arai, M. Hydrogenation of nitrobenzene with supported platinum catalysts in supercritical carbon dioxide: Effects of pressure, solvent, and metal particle size. *J. Catal.* **2004**, *224*, 479–483.
[38] Mondal, B.; Mukherjee, P. S. Cage encapsulated gold nanoparticles as heterogeneous photocatalyst for facile and selective reduction of nitroarenes to azo compounds. *J. Am. Chem. Soc.* **2018**, *140*, 12592–12601.
[39] Yang, X. F.; Wang, A. Q.; Qiao, B. T.; Li, J.; Liu, J. Y.; Zhang, T. Single-atom catalysts: A new frontier in heterogeneous catalysis. *Acc. Chem. Res.* **2013**, *46*, 1740–1748.
[40] Qiao, B. T.; Wang, A. Q.; Yang, X. F.; Allard, L. F.; Jiang, Z.; Cui, Y. T.; Liu, J. Y.; Li, J.; Zhang, T. Single-atom catalysis of CO oxidation using Pt_1/FeO_x. *Nat. Chem.* **2011**, *3*, 634–641.
[41] Jia, Y.; Zhang, L. Z.; Gao, G. P.; Chen, H.; Wang, B.; Zhou, J. Z.; Soo, M. T.; Hong, M.; Yan, X. C.; Qian, G. R. et al. A heterostructure coupling of exfoliated Ni–Fe hydroxide nanosheet and defective graphene as a bifunctional electrocatalyst for overall water splitting. *Adv. Mater.* **2017**, *29*, 1700017.
[42] Ling, C. Y.; Shi, L.; Ouyang, Y. X.; Zeng, X. C.; Wang, J. L. Nanosheet supported single-metal atom bifunctional catalyst for overall water splitting. *Nano Lett.* **2017**, *17*, 5133–5139.
[43] He, T. W.; Zhang, C. M.; Du, A. J. Single-atom supported on graphene grain boundary as an efficient electrocatalyst for hydrogen evolution reaction. *Chem. Eng. Sci.* **2019**, *194*, 58–63.
[44] He, T. W.; Matta, S. K.; Will, G.; Du, A. J. Transition-metal single atoms anchored on graphdiyne as high-efficiency electrocatalysts for water splitting and oxygen reduction. *Small Methods* **2019**, in press, https://doi.org/10.1002/smtd.201800419.
[45] Fei, H. L.; Dong, J. C.; Feng, Y. X.; Allen, C. S.; Wan, C. Z.; Volosskiy, B.; Li, M. F.; Zhao, Z. P.; Wang, Y. L.; Sun, H. T. et al. General synthesis and definitive structural identification of MN_4C_4 single-atom catalysts with tunable electrocatalytic activities. *Nat. Catal.* **2018**, *1*, 63–72.
[46] He, T. W.; Zhang, C. M.; Will, G.; Du, A. J. Cobalt porphyrin supported on graphene/Ni (111) surface: Enhanced oxygen evolution/reduction reaction and the role of electron coupling. *Catal. Today* **2018**, in press, https://doi.org/10.1016/j.cattod.2018.10.056.
[47] Lin, Z. Z. Graphdiyne-supported single-atom Sc and Ti catalysts for high-efficient CO oxidation. *Carbon* **2016**, *108*, 343–350.
[48] Back, S.; Lim, J.; Kim, N. Y.; Kim, Y. H.; Jung, Y. Single-atom catalysts for CO_2 electroreduction with significant activity and selectivity improvements. *Chem. Sci.* **2017**, *8*, 1090–1096.
[49] Yandulov, D. V.; Schrock, R. R. Catalytic reduction of dinitrogen to ammonia at a single molybdenum center. *Science* **2003**, *301*, 76–78.
[50] He, T. W.; Matta, S. K.; Du, A. J. Single tungsten atom supported on N-doped graphyne as a high-performance electrocatalyst for nitrogen fixation under ambient conditions. *Phys. Chem. Chem. Phys.* **2019**, *21*, 1546–1551.
[51] Wei, H. S.; Liu, X. Y.; Wang, A. Q.; Zhang, L. L.; Qiao, B. T.; Yang, X. F.; Huang, Y. Q.; Miao, S.; Liu, J. Y.; Zhang, T. FeO_x-supported platinum single-atom and pseudo-single-atom catalysts for chemoselective hydrogenation of functionalized nitroarenes. *Nat. Commun.* **2014**, *5*, 5634.
[52] Huang, F.; Deng, Y. C.; Chen, Y. L.; Cai, X. B.; Peng, M.; Jia, Z. M.; Ren, P. J.; Xiao, D. Q.; Wen, X. D.; Wang, N. et al. Atomically dispersed Pd on nanodiamond/graphene hybrid for selective hydrogenation of acetylene. *J. Am. Chem. Soc.* **2018**, *140*, 13142–13146.
[53] Liu, J.; Liu, Y.; Liu, N. Y.; Han, Y. Z.; Zhang, X.; Huang, H.; Lifshitz, Y.; Lee, S. T.; Zhong, J.; Kang, Z. H. Metal-free efficient photocatalyst for stable visible water splitting via a two-electron pathway. *Science* **2015**, *347*, 970–974.
[54] Zheng, Y.; Jiao, Y.; Zhu, Y. H.; Li, L. H.; Han, Y.; Chen, Y.; Du, A. J.; Jaroniec, M.; Qiao, S. Z. Hydrogen evolution by a metal-free electrocatalyst. *Nat. Commun.* **2014**, *5*, 3783.
[55] Gao, G. P.; Jiao, Y.; Waclawik, E. R.; Du, A. J. Single atom (Pd/Pt) supported on graphitic carbon nitride as an efficient photocatalyst for visible-light reduction of carbon dioxide. *J. Am. Chem. Soc.* **2016**, *138*, 6292–6297.
[56] Li, X. G.; Bi, W. T.; Zhang, L.; Tao, S.; Chu, W. S.; Zhang, Q.; Luo, Y.; Wu, C. Z.; Xie, Y. Single-atom Pt as Co-catalyst for enhanced photocatalytic H_2 evolution. *Adv. Mater.* **2016**, *28*, 2427–2431.
[57] Chen, G. X.; Xu, C. F.; Huang, X. Q.; Ye, J. Y.; Gu, L.; Li, G.; Tang, Z. C.; Wu, B. H.; Yang, H. Y.; Zhao, Z. P. et al. Interfacial electronic effects control the reaction selectivity of platinum catalysts. *Nat. Mater.* **2016**, *15*, 564.
[58] Gong, L.; Mu, Y.; Janik, M. J. Mechanistic roles of catalyst surface coating in nitrobenzene selective reduction: A first-principles study. *Appl. Catal. B: Environ.* **2018**, *236*, 509–517.
[59] Sheng, T.; Qi, Y. J.; Lin, X.; Hu, P.; Sun, S. G.; Lin, W. F. Insights into the mechanism of nitrobenzene reduction to aniline over Pt catalyst and the significance of the adsorption of phenyl group on kinetics. *Chem. Eng. J.* **2016**, *293*, 337–344.
[60] Kresse, G.; Joubert, D. From ultrasoft pseudopotentials to the projector augmented-wave method. *Phys. Rev. B* **1999**, *59*, 1758–1775.
[61] Kresse, G.; Furthmüller, J. Efficient iterative schemes for *ab initio* total-energy calculations using a plane-wave basis set. *Phys. Rev. B* **1996**, *54*, 11169–11186.
[62] Perdew, J. P.; Burke, K.; Ernzerhof, M. Generalized gradient approximation made simple. *Phys. Rev. Lett.* **1996**, *77*, 3865–3868.
[63] Henkelman, G.; Uberuaga, B. P.; Jónsson, H. A climbing image nudged elastic band method for finding saddle points and minimum energy paths. *J. Chem. Phys.* **2000**, *113*, 9901–9904.
[64] Henkelman, G.; Jónsson, H. Improved tangent estimate in the nudged elastic band method for finding minimum energy paths and saddle points. *J. Chem. Phys.* **2000**, *113*, 9978–9985.
[65] Vilé, G.; Albani, D.; Nachtegaal, M.; Chen, Z. P.; Dontsova, D.; Antonietti, M.; López, N.; Pérez-Ramírez, J. A stable single-site palladium catalyst for hydrogenations. *Angew. Chem., Int. Ed.* **2015**, *54*, 11265–11269.
[66] Boronat, M.; Concepción, P.; Corma, A.; González, S.; Illas, F.; Serna, P. A molecular mechanism for the chemoselective hydrogenation of substituted nitroaromatics with nanoparticles of gold on TiO_2 catalysts: A cooperative effect between gold and the support. *J. Am. Chem. Soc.* **2007**, *129*, 16230–16237.
[67] Saeys, M.; Reyniers, M. F.; Marin, G. B.; Neurock, M. Density functional study of benzene adsorption on Pt (111). *J. Phys. Chem. B* **2002**, *106*, 7489–7498.
[68] Saeys, M.; Reyniers, M. F.; Neurock, M.; Marin, G.; Marin G. B. *Ab initio* reaction path analysis of benzene hydrogenation to cyclohexane on Pt (111). *J. Phys. Chem. B* **2005**, *109*, 2064–2073.
[69] He, T. W.; Gao, G. P.; Kou, L. Z.; Will, G.; Du, A. J. Endohedral metallofullerenes (M@C60) as efficient catalysts for highly active hydrogen evolution reaction. *J. Catal.* **2017**, *354*, 231–235.
[70] Wang, H. T.; Xu, S. C.; Tsai, C.; Li, Y. Z.; Liu, C.; Zhao, J.; Liu, Y. Y.; Yuan, H. Y.; Abild-Pedersen, F.; Prinz, F. B. et al. Direct and continuous strain control of catalysts with tunable battery electrode materials. *Science* **2016**, *354*, 1031–1036.
[71] Mahata, A.; Rai, R. K.; Choudhuri, I.; Singh, S. K.; Pathak, B. Direct vs. Indirect pathway for nitrobenzene reduction reaction on a Ni catalyst surface: A density functional study. *Phys. Chem. Chem. Phys.* **2014**, *16*,

26365–26374.
[72] Millán, R.; Liu, L. C.; Boronat, M.; Corma, A. A new molecular pathway allows the chemoselective reduction of nitroaromatics on non-noble metal catalysts. *J. Catal*. **2018**, *364*, 19–30.
[73] Xia, L. X.; Li, D.; Long, J.; Huang, F.; Yang, L. N.; Guo, Y. S.; Jia, Z. M.; Xiao, J. P.; Liu, H. Y. N-doped graphene confined Pt nanoparticles for efficient semi-hydrogenation of phenylacetylene. *Carbon* **2019**, *145*, 47–52.
[74] Tafesh, A. M.; Weiguny, J. A review of the selective catalytic reduction of aromatic nitro compounds into aromatic amines, isocyanates, carbamates, and ureas using CO. *Chem*. *Rev*. **1996**, *96*, 2035–2052.
[75] Liao, G. Z.; Chen, S.; Quan, X.; Yu, H. T.; Zhao, H. M. Graphene oxide modified g-C_3N_4 hybrid with enhanced photocatalytic capability under visible light irradiation. *J*. *Mater*. *Chem*. **2012**, *22*, 2721–2726.
[76] Liu, S. Z.; Ke, J.; Sun, H. Q.; Liu, J.; Tade, M. O.; Wang, S. B. Size dependence of uniformed carbon spheres in promoting graphitic carbon nitride toward enhanced photocatalysis. *Appl*. *Catal*. *B*: *Environ*. **2017**, *204*, 358–364.
[77] Zhang, X. D.; Xie, X.; Wang, H.; Zhang, J. J.; Pan, B. C.; Xie, Y. Enhanced photoresponsive ultrathin graphitic-phase C_3N_4 nanosheets for bioimaging. *J*. *Am*. *Chem*. *Soc*. **2012**, *135*, 18–21.